Quantum decoherence of I_2 in liquid xenon: A classical Wigner approach

Cite as: J. Chem. Phys. **138**, 234308 (2013); https://doi.org/10.1063/1.4810009
Submitted: 07 April 2013 • Accepted: 28 May 2013 • Published Online: 19 June 2013

Yossi Elran and Paul Brumer

Quantum decoherence of I_2 in liquid xenon: A classical Wigner approach

Yossi Elran[a] and Paul Brumer[b]
Chemical Physics Theory Group, Department of Chemistry, and Centre for Quantum Information and Quantum Control, University of Toronto, Toronto, Ontario M5S 3H6, Canada

(Received 7 April 2013; accepted 28 May 2013; published online 19 June 2013)

Vibrational decoherence of a "breathing sphere" oscillator in a thermal Lennard-Jones bath is examined using a classical analog approach. The equivalence between this approach and the linearized semiclassical initial value representation (IVR) is established and the method is exploited to produce a useful computational strategy that can efficiently evaluate the time dependence of the decoherence in these systems. A comparison between Harmonic and Morse "breathing sphere" models is presented and the rate of decoherence is found to depend on the choice of model, the initial state of the oscillator, the initial conditions of the bath (temperature, density), and the choice of quantity measuring the decoherence rate. The results are used to examine the utility of the Caldeira-Leggett model in this realistic system. © *2013 AIP Publishing LLC*. [http://dx.doi.org/10.1063/1.4810009]

I. INTRODUCTION

There has recently been growing interest in studying the role of quantum mechanics in large open systems. One effect of considerable importance is decoherence, the loss of quantum phase information as a result of coupling between a subsystem, which is of interest, and the environment, which is not. Interest in this process arises from a crucial role that decoherence plays in the transition from quantum and classical behavior,[1–4] and in its negative influence on any process reliant upon quantum coherence effects, such as quantum computation[5] or quantum control of atomic and molecular processes.[6–8] Decoherence is also central to the chemistry of reactions in solution[9,10] and is the first step in the generic vibrational relaxation process of a molecule in the condensed phase. In addition, issues of quantum decoherence have become of increasing interest due to the observation of long-lived coherences in nanosystems that are relevant in natural light harvesting, e.g., photosynthesis.[11–14]

Consider a system comprising a subsystem coupled to a bath. The time evolution of the system density matrix ρ satisfies the Liouville-von Neumann equation:[15]

$$\frac{d\rho}{dt} = -i/\hbar[H, \rho] \equiv L\rho, \tag{1}$$

where H is the total Hamiltonian, $H = H_s + H_B + H_{sB}$, i.e., the sum of subsystem H_s, bath H_B and subsystem-bath coupling H_{sB} Hamiltonian. The Liouville operator L is defined by this equation. Below the eigenstates and eigenvalues of H_s are denoted $|\psi_i\rangle$ and E_i.

The subsystem dynamics is obtained by tracing ρ over the bath degrees of freedom, giving a generalized master equation for the non-unitary time evolution of the reduced density operator ρ_s of the subsystem.[16] Often, theoretical studies of decoherence utilize models[17] derived from this generalized master equation, obtained by introducing various approximations, such as Markovian dynamics, weak coupling, etc. For example, the Caldeira-Leggett, Redfield and Lindblad master equations are popular, and have afforded considerable insight into the physics of decoherence.[4] Nonetheless, these models do not necessarily describe the actual dynamics that occur in a *specific* chemical or physical situation. For example, our earlier semiclassical study[18] of diatomic vibrational decoherence in an harmonic bath showed that these models were qualitatively inaccurate, as was a recent study of Markovian master equations in photosynthetic systems.[19]

In this paper, we examine decoherence in a realistic model, I_2 in a Xe bath, by computing the full dynamics of ρ, and hence of ρ_s. An exact quantum calculation of this kind is beyond computational capabilities, and may well be unnecessary. That is, our recent work[20] shows analytically that, under rather well defined conditions, the classical analogue (CA) approach described below gives accurate short time results for decoherence dynamics. In this approach, the initial quantum state of a system is described by the Wigner distribution while the subsequent time evolution is carried out classically. In phase space regions where the initial Wigner distribution is negative, the classical trajectories carry this negative weight. Additional computational work[9] supports the utility of the method over all times. Further, the approach is shown, in the Appendix, to give results that are equivalent to the linearized semiclassical initial value representation (IVR) method. Conditions under which this approach is unreliable have recently been discussed.[2] However, for the quantities described below, ample proof has been provided[20] for the accuracy of this method.

The classical analogue approach that we advocate has a long history,[21] having emanated from various distinct perspectives. However, it is useful to comment on the origins of the classical analogue perspective; we do so in the first part of Sec. II. We believe that this formal approach provides useful insights into the origins of the CA.

[a]Present address: Davidson Institute of Science Education, Weizmann Institute of Science, P.O. Box 26, Rehovot 76200, Israel.
[b]Author to whom correspondence should be addressed. Electronic mail: pbrumer@chem.utoronto.ca

In the study below we consider decoherence of vibrational motion in a liquid solvent. Specifically, we examine the case of I_2 superposition states evolving in thermal liquid Xe, with an ensemble of classical particles distributed according to a Wigner distribution, and the total system propagated classically. A number of interesting questions regarding decoherence are addressed. What is the time scale of decoherence in these systems? How do the initial conditions, both of the bath and the system, effect decoherence? Do sample model master equations predict the correct behavior of a real system undergoing decoherence, and if so, can we use CA calculations to predict the value of (arbitrary) parameters that appear in these equations?

This paper is organized as follows: Section II introduces the basic formulas for the quantities that are used to describe decoherence. In Sec. III we discuss the computational application to a subsystem-bath scenario. Section IV contains a discussion of the results and finally, in Sec. V we summarize. For convenience, the phrase "density matrix," for the remainder of this paper, refers to the reduced density matrix ρ_s of the subsystem.

II. CLASSICAL ANALOG METHODOLOGY FOR DECOHERENCE

The literature proposes several measures of the subsystem decoherence. Here we adopt two, the dynamics of (a) the purity of the reduced density matrix $\mathrm{Tr}_s(\rho_s^2)$, and (b) the off-diagonal elements of the density matrix $\langle\psi_i|\rho_s|\psi_j\rangle$, where the $|\psi_i\rangle$ are eigenstates of H_s.

Below we introduce the basic CA formulae for these two quantities. In addition, other measures of decoherence related to the Caldeira-Leggett model for the time-dependent density operator are discussed. Below, the use of the term "Tr" without any subscript denotes a trace over the full system variables, Tr_B denotes a trace over the bath, and Tr_s denotes a trace over the subsystem variables.

A. The purity $\mathrm{Tr}_s(\rho_s^2)$

In the absence of decoherence, $\mathrm{Tr}_s(\rho_s^2) = \mathrm{Tr}_s(\rho_s) = 1$, whereas in the presence of decoherence, $\mathrm{Tr}_s(\rho_s^2) < 1$, and reaches $\mathrm{Tr}_s(\rho_s^2) = \sum_i \exp[-2\beta E_i]/[\sum_j e^{-\beta E_j}]^2$ when the system is in thermal equilibrium with an external bath at temperature T.

Consider then the time evolution of $\rho_s(t)$, given an initial density $\rho(0)$

$$\rho_s(t) = \mathrm{Tr}_B[e^{-iLt}\rho(0)] = \mathrm{Tr}_B[e^{iHt}\rho(0)e^{-iHt}], \tag{2}$$

where L is the Liouville operator defined in Eq. (1). Average values, $\langle C(t)\rangle$, of properties C at time t are given by

$$\langle C(t)\rangle = \mathrm{Tr}_s[C\rho_s(t)] = \mathrm{Tr}[C(e^{iHt}\rho(0)e^{-iHt})]. \tag{3}$$

Note that cyclic invariance of the trace implies that

$$\langle C(t)\rangle = \mathrm{Tr}[(e^{-iHt}Ce^{iHt})\rho(0)] = \mathrm{Tr}[C(t)\rho(0)], \tag{4}$$

so that we may either propagate ρ or C in time in order to obtain the time average of C at time t.

For use below, we note that Eq. (3) can be written in the Wigner representation as

$$\langle C(t)\rangle = \int dx_s dx_B C_w(x_s, x_B, 0)\rho^w(x_s, x_B, t), \tag{5}$$

where x_s and x_B are the multidimensional coordinates and momenta of the subsystem and bath, respectively, and where $C_w(x_s, x_B, 0)$ and $\rho^w(x_s, x_B, t)$ are the Wigner representations of $C(t = 0)$ and of $\rho(t)$.

The exact time evolution of $\rho^w(x_s, x_B, t)$ can be obtained by solving Eq. (1) in the Wigner representation, i.e.,

$$\begin{aligned}\frac{d\rho^w(x_s, x_B, t)}{dt} &= -\{\{\rho^w(x_s, x_B, t), H\}\} \\ &= -\{\rho^w(x_s, x_B, t), H\} + \mathcal{O}(\hbar^2),\end{aligned} \tag{6}$$

where $\{\{,\}\}$ denotes the Moyal bracket and $\{,\}$ denotes the Poisson bracket. The classical approximation (CA) adopted below, consists of propagating $\rho^w(x_s, x_B, t)$ using only the first term on the right hand side of Eq. (6), i.e., $\rho^w(x_s, x_B, t)$ is propagated purely classically. Quantum features then appear solely through the negative values that $\rho^w(x_s, x_B, t)$ may assume at $t = 0$. In the case where Eq. (6) is solved by the method of characteristics, i.e., by propagating trajectories with weights given by $\rho^w(x_s, x_B, 0)$, then the trajectories are weighted with negative values if they emanate from an initial phase space point x_s, x_B where $\rho^w(x_s, x_B, 0)$ is negative. The demonstration that this approach is the same as the linearized semiclassical IVR method is provided in the Appendix. However, the implementation of the CA, as described below, is considerably more efficient than is the traditional implementation of the linearized semiclassical IVR method. This added efficiency, as discussed in the Appendix, is due to the absence of phase factors in this approach, and the method of "boxing" the trajectories.

Consider, for example, the direct quantum computation of the purity $\mathrm{Tr}_s(\rho_s^2(t))$, which is given by

$$\mathrm{Tr}_s\left(\rho_s^2(t)\right) = \int dx_s \left[\int dx_B \rho^w(x_s, x_B, t)\right]^2. \tag{7}$$

Inserting unity in the form of a delta-function in the system variables gives

$$\mathrm{Tr}_s\left(\rho_s^2(t)\right) = \int dx_s \left[\int dx_s' dx_B \delta(x_s' - x_s)\rho^w(x_s, x_B, t)\right]^2, \tag{8}$$

$$\mathrm{Tr}_s\left(\rho_s^2(t)\right) = \int dx_s \left[\int dx_s' dx_B \delta(x_s' - x_s)e^{-iL_w t}\rho^w(x_s, x_B, 0)\right]^2. \tag{9}$$

The Liouville operator can now be moved to operate on the delta-function

$$\begin{aligned}&\mathrm{Tr}_s\left(\rho_s^2(t)\right) \\ &= \int dx_s \left[\int dx_s' dx_B [e^{iL_w t}\delta(x_s' - x_s)]\rho^w(x_s, x_B, 0)\right]^2,\end{aligned} \tag{10}$$

giving

$$\mathrm{Tr}_s\left(\rho_s^2(t)\right) = \int dx_s \left[\int dx_s' dx_B \delta(x_s'(t) - x_s)\rho^w(x_s, x_B, 0)\right]^2. \tag{11}$$

Here $x_s'(t)$ are the subsystem coordinates and momenta that result, at time t, from trajectory propagation that began at the point x_s' at time zero. Needless to say, obtaining $x_s'(t)$ requires propagating the entire coupled subsystem and bath.

We assume separable initial conditions, i.e., that the initial state is given by $\rho(x_s, x_B, 0) = \rho_s(x_s, 0) \times \rho_B(x_B, 0)$. This permits an assessment of the rate of decoherence induced as the system and bath become entangled. Further, the initial bath density ρ_B is taken as a canonical (NVT) ensemble at conditions under which the Xe is a liquid. The initial system density ρ_s is chosen as a Wigner transform of the selected initial state of the system. We consider a variety of different initial states including coherent states and superposition states, as described below.

Evaluation of Eq. (11) is best carried out using Monte Carlo integration,

$$\mathrm{Tr}\left(\rho_s^2(t)\right) = \int dx_s \left[\int dx_s' dx_B \delta(x_s'(t) - x_s)\frac{\rho(x_s, x_B, 0)}{W(x_s, x_B)} W(x_s, x_B)\right]^2, \tag{12}$$

where the sampling is performed using a useful distribution function $W(x_s, x_B)$. Choosing the bath component of $W(x_s, x_B)$ to be the canonical ensemble ρ_B and assuming $W(x_s, x_B) = W(x_s)W(x_B)$ the Monte Carlo summation can be written as

$$\mathrm{Tr}\left(\rho_s^2(t)\right) = \int dx_s \left[\frac{1}{N}\sum_{i=1}^{N} \delta(x_s'(t) - x_s)\frac{\rho_s(x_s, 0)}{W(x_s)}\right]^2 \equiv \int dx_s \rho_s(x_s, t)^2, \tag{13}$$

where $\rho_s(x_s, 0)$ describes the subsystem states at time zero and points are selected from $W(x_s, x_B)$.

If the initial subsystem density $\rho_s(x_s, 0)$ is a coherent state, the integration in Eq. (11) can readily be performed using Monte Carlo importance sampling with the x_s points weighted by $\rho(x_s, 0)$:

$$\mathrm{Tr}\left(\rho_s^2(t)\right) \equiv \int dx_s \rho_s(x_s, t)^2 = \int dx_s \left[\frac{1}{N}\sum_{i=1}^{N} \delta(x_s'(t) - x_s)\right]^2. \tag{14}$$

In the Appendix, we show that Eq. (11) is equivalent to the LSC-IVR, although computationally easier to compute.

B. Off-diagonal matrix elements

The linear entropy $\mathrm{Tr}(\rho_s^2(t))$ is one useful, basis independent measure of the rate at which coherence is lost to the subsystem. Also of interest is the rate at which the subsystem off-diagonal matrix elements decay in the subsystem energy representation, given by[20]

$$\rho_{ij}(t) = \langle\psi_j|\rho_s|\psi_i\rangle = \mathrm{Tr}[\rho_s(t)|\psi_i\rangle\langle\psi_j] = \mathrm{Tr}[\rho_s(x_s, t)(|\psi_i\rangle\langle\psi_j|)_w]. \tag{15}$$

Here, $(|\psi_i\rangle\langle\psi_j|)_w$ denotes the Wigner function for the operator in the subsystem energy basis. Given that our subsystem below is one-dimensional (the vibrational coordinate of I_2), we denote its coordinate and momentum as q, p.

The relationship between $\rho_{ij}(t)$ and the evolution of $\mathrm{Tr}_s(\rho_s^2(t))$ is straightforward

$$\mathrm{Tr}_s\left(\rho_s^2(t)\right) = \sum_{jk} |\rho_{jk}|^2 = \sum_j |\rho_{jj}|^2 + \sum_{i\neq j} |\rho_{ij}|^2. \tag{16}$$

Hence, $\mathrm{Tr}_s(\rho_s^2(t))$ contains contributions from both relaxation (via $\rho_{jj}(t)$) and the collective phase loss (via $\rho_{ij}(t)$) of all levels.

Using the classically propagated expression for $\rho_s(x_s, t)$ and the quantum expression for $(|\psi_i\rangle\langle\psi_j|)_w$:

$$(|\psi_i\rangle\langle\psi_j|)_w = \frac{1}{2\pi\hbar}\int_{-\infty}^{\infty} dy e^{\frac{ipy}{\hbar}}\left\langle q - \frac{y}{2}|\psi_i\rangle\langle\psi_j|q + \frac{y}{2}\right\rangle \tag{17}$$

gives the classical analog approximation[21] to $\rho_{ij}(t)$. Specifically, we have

$$\rho_{ij}(t) = \frac{1}{2\pi\hbar}\int dx_s dy e^{\frac{ipy}{\hbar}}\left\langle q - \frac{y}{2}|\psi_i\rangle\langle\psi_j|q + \frac{y}{2}\right\rangle \rho_s(x_s, t), \tag{18}$$

where the $|\psi_i\rangle$ are the vibrational eigenstates of the I_2 molecule. Two different models are considered below: the more accurate Morse function eigenstates, and the approximate harmonic eigenstates. They will be seen to give remarkably different decoherence results.

Equations (13), (14) and (18) are all that is required to calculate the quantities of interest. No assumptions were made with respect to the system, the bath or initial conditions, except that at time $t = 0$ the bath and system are separable.

C. Caldeira-Leggett model

Many master equations for the subsystem density matrix have been proposed which rely on assumptions made for the subsystem, the bath and the initial conditions. One such approach is the Markovian Caldeira-Leggett model that considers a Hamiltonian subsystem coupled to a bath of harmonic oscillators via linear coupling in the high temperature, low coupling limit. Below, as before,[18] we examine the utility of this master equation as compared to the classical analog results. A simple test of the utility of this model can be established. Specifically, the rate of decay of the Renyi entropy, $S = \ln(\mathrm{Tr}[(\rho^w)^2])$, is directly related to the purity and is given for the Caldeira-Leggett model by[22]

$$\frac{dS}{dt} = 2D\frac{\mathrm{Tr}\left[\rho^w \frac{\partial^2 \rho^w}{\partial p^2}\right]}{\mathrm{Tr}[(\rho^w)^2]} \equiv -2D\chi^2, \tag{19}$$

where ρ^w is the subsystem Wigner density. The parameter D of the Caldeira-Leggett model depends monotonically on the coupling and temperature of the environment, with the standard form for coordinate coupling being $D = 2\gamma M k_B T$ where T is the temperature of the bath, γ is a measure of the system-environment coupling, k_B is the Boltzmann constant and M is the system mass. The quantity χ^2 is a measure of the structure in momentum space, averaged over all the coordinates and is implicitly defined in Eq. (19):

$$\chi^2 = -\frac{\mathrm{Tr}\left[\rho^w \frac{\partial^2 \rho^w}{\partial p^2}\right]}{\mathrm{Tr}\left[(\rho^w)^2\right]}. \tag{20}$$

Note that here, unlike Ref. 23, we use the second derivative with respect to the momentum, rather than derivatives with respect to both coordinates and momenta, since the system-bath coupling adopted here depends only on the coordinate. A detailed explanation of the physical interpretation of χ^2 was given in Ref. 18. Although discussed here specifically for the Caldeira-Leggett model, its physical interpretation is model independent and is a useful quantity for studying decoherence. In the Caldeira-Leggett model χ^2 is a positive real number since $\frac{dS}{dt}$ is negative definite.

The classical analog approximation to χ^2 is obtained from Eqs. (18) and (20) as

$$\chi^2(t) = \frac{-1}{2\pi} \sum_{i,j,k,l} \int_{-\infty}^{\infty} dq\, dy\, y^2 \left\langle q - \frac{y}{2}|\psi_i\rangle \rho_{ij}(t) \langle \psi_j|q + \frac{y}{2}\right\rangle \times \left\langle q + \frac{y}{2}|\psi_k\rangle \rho_{kl}(t) \langle \psi_l|q - \frac{y}{2}\right\rangle. \tag{21}$$

Computing $\chi^2(t)$ enables an independent calculation of D from the relationship

$$D = -\frac{dS}{dt} \Big/ (2\chi^2). \tag{22}$$

If D is constant, that is, independent of time and of initial ρ_s, then it confirms the possible utility of the Caldeira-Leggett equation, as well as providing a value of the unknown D, and hence γ.

III. APPLICATION TO I_2 IN LIQUID Xe

A. Computational details

Consider now the application of this approach to a realistic subsystem-bath scenario; a single diatomic solute immersed in a monatomic fluid. The vibrational relaxation rate of this system has been studied extensively.[24] The total (quantum-mechanical) Hamiltonian for a diatomic oscillator in a bath of N particles is

$$H = \frac{p^2}{2\mu} + V(q) + \frac{P_0^2}{2m_0} + \sum_{i=1}^{N} \phi(r_{i0}, q) + \sum_{j=1}^{N} \frac{P_j^2}{2M_B} + \sum_{i<j}^{f-1} \phi_B(r_{ij}). \tag{23}$$

Here (p, q) are the system vibrational phase space variables with reduced mass μ and potential $V(q)$. The solute is assumed to be a "breathing sphere" of mass m_0, P_0 is the sphere's translational momentum and $\phi(r_{i0}, q)$ is the solute-solvent pair potential, with r_{i0} the distance between the ith solvent atom and the diatomic. The mass of the solvent atoms is M_B, P_j is the translational momentum of the jth solvent atom and $\phi_B(r_{ij})$ is the solvent-solvent pair potential with r_{ij} the distance between the ith and jth solvent atoms.

Here we consider the specific case of an iodine molecule immersed in a bath of xenon atoms. Two sample vibrational potentials for the iodine molecule are considered: an harmonic oscillator with $V(q) = \mu\omega^2/2$ and the more realistic Morse potential: $V(x) = D[1 - e^{-a(q-q_e)}]^2$. The potential parameters used correspond to the ground electronic state of molecular iodine: $D = 1.2547 \times 10^4$ cm^{-1}, $x_e = 2.6663$ Å, $a = 1.8576$ Å^{-1}, $\mu = 0.06345$ Kg/mol, and $\omega = 2.137 \times 10^{-6}$ Å^{-1}. The pairwise interactions between the solute and the solvent and between the solvent atoms are Lennard-Jones potentials given by

$$\phi(r_{i0}, q) = 4\sqrt{\epsilon_0 \epsilon_s}\left[\left(\frac{\sigma_s + \sigma_0 + \alpha q}{2r_{i0}}\right)^{12} - \left(\frac{\sigma_s + \sigma_0 + \alpha q}{2r_{i0}}\right)^{6}\right],$$

$$\phi_B(r_{ij}) = 4\epsilon_s\left[\left(\frac{\sigma_B}{2r_{ij}}\right)^{12} - \left(\frac{\sigma_B}{2r_{ij}}\right)^{6}\right],$$

where ϵ_0 and ϵ_s are the solute-solute and solvent-solvent respective well depths, σ_B and σ_0 are the solute and solvent effective diameters and α is a dimensionless parameter that adjusts the diameter of the effective breathing sphere. Previous relaxation studies[24] comparing theory and experiment suggest that $\alpha = 0.7$, with $\epsilon_{I_2} = \epsilon_0 = 550$ K, $\epsilon_{Xe} = \epsilon_s = 221.7$ K, $\sigma_{I_2} = \sigma_0 = 4.982$ Å, and $\sigma_{Xe} = \sigma_s = 3.93$ Å, the values used below.

Computationally, the evaluation of the purity via Eqs. (12)–(14) can be interpreted in the following manner: sample the initial conditions for the bath and the subsystem, propagate the subsystem variables x_s' under the full Hamiltonian by integrating Hamilton's equations of motion for the full system, and then "box" these time-evolved variables $x_s'(t)$ onto the subsystem's phase space grid by counting the number of variables that fall into each grid compartment dx_s at time t. If the initial state of the system is a coherent state we use Eq. (14). If it is a canonical ensemble then, each "boxed" variable is multiplied by a weight $\rho(x_s)/W(x_s)$ as in Eq. (13).

At time $t = 0$, the bath and subsystem are assumed to be separated, with the bath particle properties sampled them from a canonical distribution. Specifically, we run a Molecular Dynamics (MD) calculation. Initially, the xenon atoms in the bath are placed on a cube, the breathing sphere solute is placed arbitrarily in a vacancy in the cube and a standard MD trajectory is initiated, using the velocity-Verlet algorithm for the trajectory, periodic boundary conditions, truncated and shifted potential[25] and velocity resampling in order to ensure an accurate NVE calculation. After equilibration, canonical distributions of these particles can be selected at arbitrary time intervals, as long as these time intervals are long enough so that there are effectively no correlations between the samples. The initial system (vibrational) position and

momentum are selected randomly from the appropriate Wigner distribution.

The computational procedure can be summarized as follows:

(1) Run an MD simulation until the bath particles have equilibrated.
(2) Continue the MD simulation and, after sampling time t_s extract the positions and momenta of the bath particles and of the breathing sphere. This extracted configuration is a canonical distribution.
(3) Sample the subsystem position and momentum from the relevant Wigner distribution.
(4) Run a classical trajectory under the full Hamiltonian using the sampled subsystem and bath configurations as the initial conditions for the trajectory. The integration of Hamilton's equations is performed using the velocity-Verlet algorithm, periodic boundary conditions for the bath and shifted and truncated potentials (for the bath).
(5) At required times t, "box" the system variables to prepare a histogram.
(6) Upon convergence with a number of trajectories, the assembly of "boxes" in the system variables, i.e., the converged histogram represents the classical density $\rho_s(t)$ required for all further calculations.

The typical value of the sampling time t_s used in this work is $t_s = 5$ time steps, where each time step is 3.316 ps.

Note that effectively the scheme presented is an MC-MD calculation. The structure of the algorithm makes it very convenient to parallelize the computation, effectively reducing the overall computational load. Additionally, the propagation of the trajectories in the manner described, efficiently replaces the more tedious task of integrating complex integrands, usually invoked in semiclassical calculations.

IV. RESULTS AND DISCUSSION

Consider the vibrational decoherence of I_2 in a liquid state xenon bath at T = 222 K and at the density 3.07 g/cm^3. For calculations of relaxation rates, a bath of 864 atoms is required in order to obtain accurate results.

For the case of a coherent initial vibrational state, a total number of 10 000 trajectories and a phase space grid of 100 gridpoints are needed for convergence. The results are accurate to within 1% for the purity and within 10% for individual ρ_{ij}. Initial vibrational superposition states were also studied. It proved much harder to achieve convergence for these cases due to the more complex structure of the initial states. Specifically, for calculations of the purity a total of 50 000 trajectories are needed with a phase space grid of 100 points. Individual density matrix elements require between 50 000 and 500 000 and a phase space grid of between 100 and 1000 points, depending on the energy level of the state; the higher the state, the larger the number of trajectories and grid size required for convergence to within an accuracy of ∼1%–3% for the purity and within ∼10%–15% for individual density matrix elements.

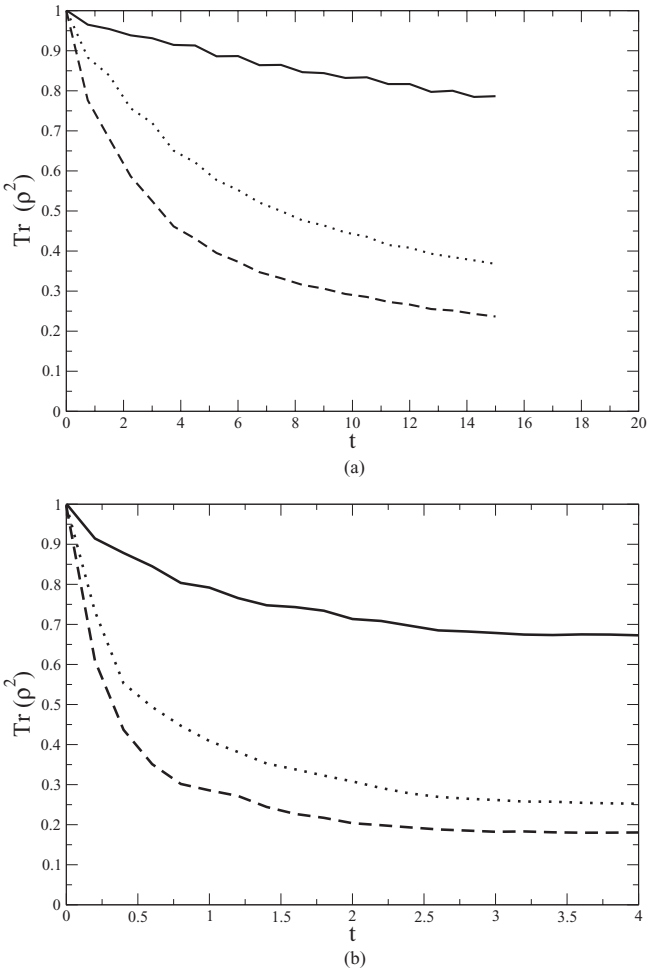

FIG. 1. (a) $\mathrm{Tr}(\rho^2)$ for a harmonic oscillator in a LJ bath as a function of time for three different initial coherent states with the initial position displacement: $q_i = 0.01$ (solid line), $q_i = 0.03$ (dotted line), $q_i = 0.05$ (dashed line). Each time unit in all figures is 3.316 ps. (b) $\mathrm{Tr}(\rho^2)$ for a Morse oscillator in a LJ bath as a function of time for three different initial coherent states with the initial position displacement: $q_i = 0.01$ (solid line), $q_i = 0.03$ (dotted line), and $q_i = 0.05$ (dashed line). Note the different ranges of the abscissa in the two figures.

A. Coherent states

Figure 1 shows the purity $\mathrm{Tr}(\rho^2)$ as a function of time for both the harmonic and Morse I_2 cases for each of three different initial coherent states described by the Wigner distribution function:

$$\rho(q, p) = \frac{1}{2\pi\hbar} \exp\left[-\frac{\mu\omega}{\hbar}(q - q_i)^2 - \frac{1}{\mu\omega\hbar}(p - p_i)^2\right] \tag{24}$$

with the initial position displacement $q_i = 0.01, 0.03, 0.05$ and initial momentum displacement $p_i = 0.0$ in all cases. One aspect of the nature of the $\rho(q, p)$ is reflected in the populations of the eigenstates $|\psi_i\rangle$ out of which it is formed, here quantified in terms of $d_i = \mathrm{Tr}[\rho(p, q)(|\psi_i\rangle\langle\psi_i|)_w]$, where $(|\psi_i\rangle\langle\psi_i|)_w$ denotes the Wigner transform of $|\psi_i\rangle\langle\psi_i|$. These d_i are shown in Fig. 2, for both the Morse and harmonic cases.

The Morse and the harmonic cases are seen to decohere on very different time scales. In particular, the timescale of decoherence for the Morse oscillator is roughly one time unit

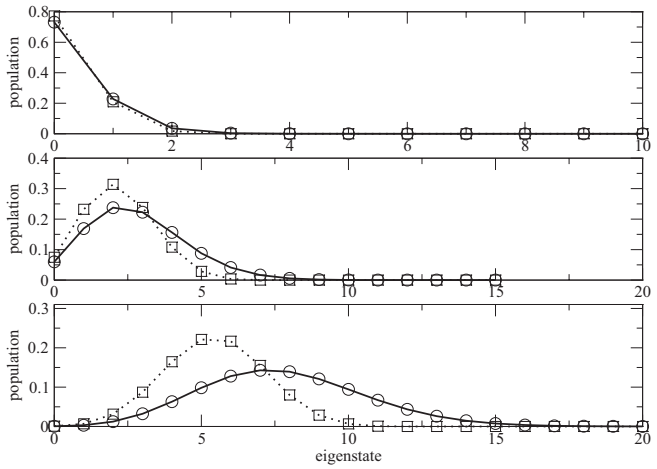

FIG. 2. Population in initial coherent states: $q_i = 0.01$ (upper pane), $q_i = 0.03$ (middle pane), $q_i = 0.05$ (lower pane), Harmonic oscillator (dotted curve), and Morse oscillator (solid curve).

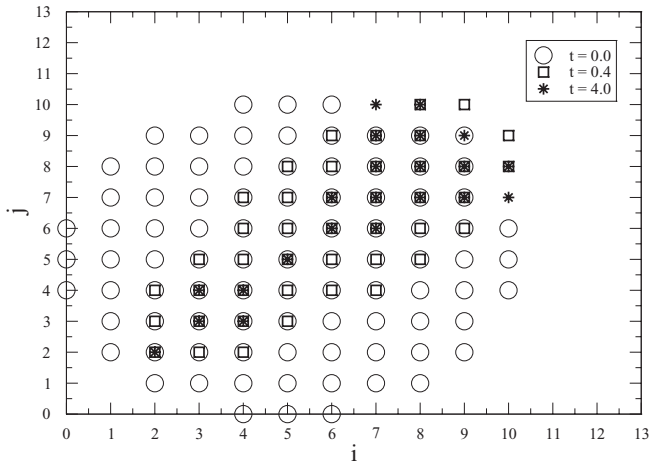

FIG. 4. Time evolution of the Morse oscillator off-diagonal density matrix elements (in the energy representation). Each point depicts a density matrix element whose absolute value is larger than the cutoff of 0.015.

(equivalent to 3.3 ps), while the timescale of decoherence for the harmonic oscillator is about eight times larger. Despite the difference in timescales, Fig. 3 shows that both the Morse and the Harmonic oscillators decay to the same asymptotic value of $\mathrm{Tr}(\rho^2)$. For example, for the initial coherent state $q_i = 0.05$, the asymptotic value of the $\mathrm{Tr}(\rho^2)$ for both the harmonic and the Morse cases is $\mathrm{Tr}\,(\rho^2) = 0.17$ and for the initial coherent state $q_i = 0.03$, the asymptotic value of $\mathrm{Tr}(\rho^2) = 0.27$. The purity is unity for a pure state and is $1/N$ for a totally incoherent mixture $\widehat{\rho} = N^{-1}\sum_{i=1,N}|i\rangle\langle i|$ of N states with equal probabilities. Given the population in Fig. 2 (roughly states are populated), one might expect the asymptotic value of the purity to be $\sim 1/N = 0.14$ for the coherent state with $q_i = 0.05$, and $\sim 1/N = 1/3 = 0.33$ for the coherent state $q_i = 0.03$. However, from Fig. 3 one sees that the long time ρ is not a statistically mixed state with equal probabilities.

Consider now the Morse oscillator case. A more general view of the time evolution of the off-diagonal density matrix elements (in the energy representation) is given in Fig. 4. Here, each point depicts a density matrix element whose absolute value is larger than the cutoff of 0.015. Results are shown at three different times. The collapse of these matrix elements towards the diagonal with time is visibly impressive. Generally speaking, the higher frequency coherences arising from levels that are widely separated decay much faster than levels that are close to one another. These results illustrate the persistence of quantum coherence for longer times than predicted by the purity.

The combination of Figures 1 and 4 makes clear that the primary decoherence process that we are seeing in Fig. 1 is the disappearance of the extreme high frequency off-diagonal components of the density matrix. Since, in accord with Eq. (25)

$$\mathrm{Tr}(\rho^2) = \sum_{i,j}\langle i|\rho|j\rangle\langle j|\rho|i\rangle = \sum_i |\langle i|\rho|i\rangle|^2 + \sum_{i\neq j}\langle i|\rho|j\rangle\langle j|\rho|i\rangle, \qquad (25)$$

the decrease of the high frequency components reduces the second term in Eq. (25), leading to a reduction in the size of $\mathrm{Tr}(\rho^2)$.

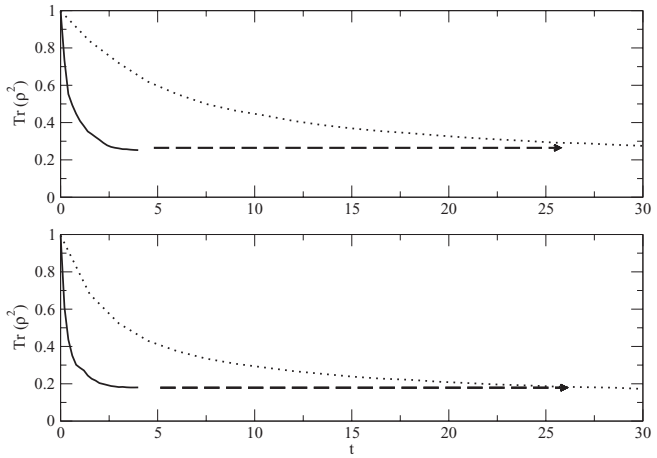

FIG. 3. Asymptotic values of the purity in initial coherent states: $q_i = 0.03$ (upper pane), $q_i = 0.05$ (lower pane), Harmonic oscillator (dotted curve), and Morse oscillator (solid curve).

B. Superposition states

Consider now the case of initial superposition states, i.e., initial states of the type $c_1\psi_1 + c_2\psi_2$; throughout we choose real coefficients with $c_1^2 = 0.4$ and $c_2^2 = 0.6$. The initial position and momentum of the diatom are sampled from the Wigner distribution function:

$$\rho^w(p,q,t) = \frac{1}{2\pi\hbar}\int_{-\infty}^{\infty} dy e^{\frac{ipy}{\hbar}}\left\langle q - \frac{y}{2}|c_1\psi_1 + c_2\psi_2\right\rangle \times\langle c_1\psi_1 + c_2\psi_2|q + \frac{y}{2}\Big\rangle.$$

Calculations were done for both the harmonic potential and the more realistic Morse potential for the diatomic. Figures 5–7 show the purity as a function of time for three

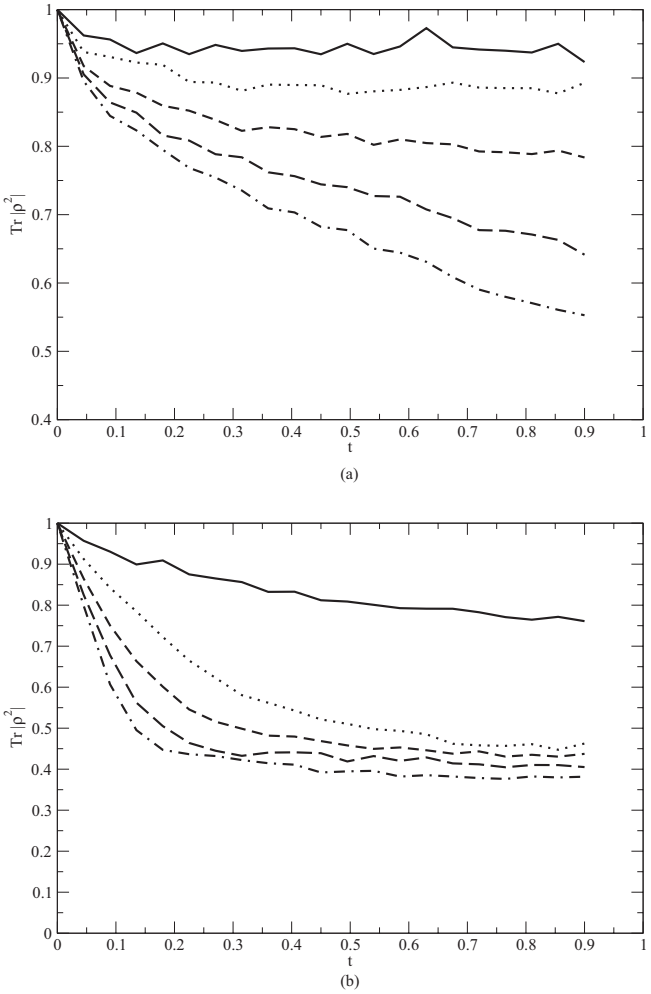

FIG. 5. (a) $\mathrm{Tr}(\rho^2)$ for a harmonic oscillator in a LJ bath as a function of time for five different initial superposition states: 0,1 (solid line); 0,2 (dotted line); 0,3 (short dashed line); 0,4 (long dashed line); 0,5 (dotted-dashed line). (b) $\mathrm{Tr}(\rho^2)$ for a morse oscillator in a LJ bath as a function of time for five different initial superposition states: 0,1 (solid line); 0,2 (dotted line); 0,3 (short dashed line); 0,4 (long dashed line); and 0,5 (dotted-dashed line).

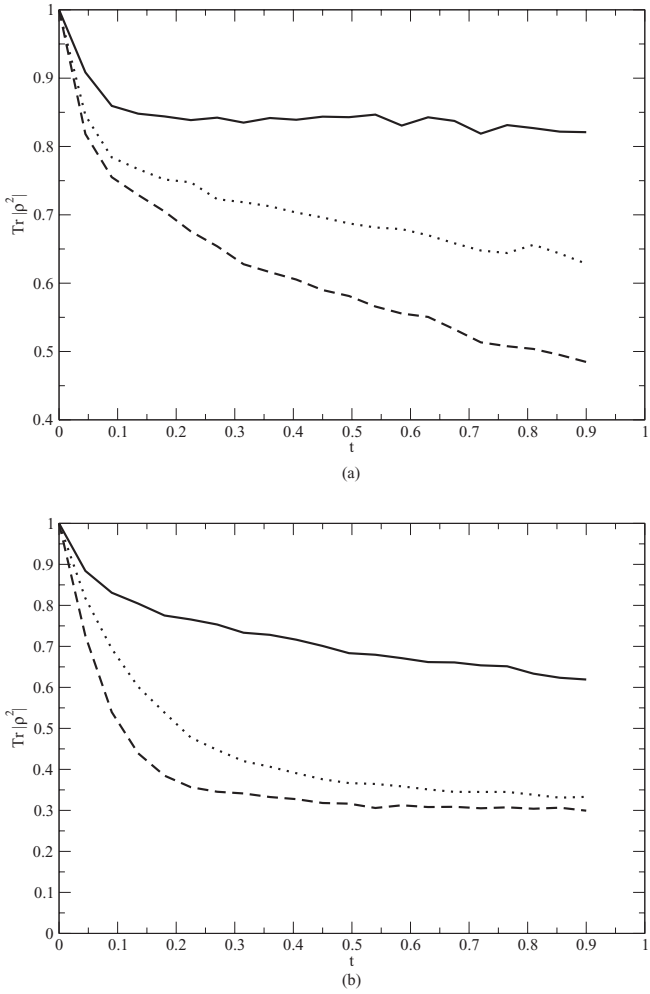

FIG. 6. (a) $\mathrm{Tr}(\rho^2)$ for a harmonic oscillator in a LJ bath as a function of time for three different initial superposition states: 3,4 (solid line); 3,6 (dotted line); 3,8 (dashed line). (b) $\mathrm{Tr}(\rho^2)$ for a Morse oscillator in a LJ bath as a function of time for three different initial superposition states: 3,4 (solid line); 3,6 (dotted line); and 3,8 (dashed line).

sets of harmonic superpositions and three sets of Morse superpositions. Specifically, the pairs considered are

Set 1: $\{(\psi_1, \psi_2)\} = \{(0, 1); (0, 2); (0, 3); (0, 4); (0, 5)\}$.
Set 2: $\{(\psi_1, \psi_2)\} = \{(3, 4); (3, 6); (3, 8)\}$.
Set 3: $\{(\psi_1, \psi_2)\} = \{(8, 9); (8, 10); (8, 11)\}$.

All curves show decay, but with much smaller decoherence timescales than those seen for coherent states. A general study of Figs. 5–7 suggests that superpositions of states of higher energies decohere faster than superpositions of low-lying states. Additionally, superpositions of states that are widely separated decohere faster than those of close-lying states, again because widely separated states have larger regions of complex structure. Note also that the asymptotic value of the $\mathrm{Tr}(\rho^2)$ at long times gives approximately the expected value of $1/N = 1/2$. In superpositions where this is not the case, this is either due to the fact that the full decoherence process takes longer than the time studied (e.g., superpositions 0, 1 and 3, 4) or because decoherence is rapid (for high energy, widely separated initial superposition states) and accompanied by population transfer processes, giving a lower than expected asymptotic values of $\mathrm{Tr}(\rho^2)$ as more than two states are involved as time progresses. One such case is superposition (0,3) wherein $\mathrm{Tr}(\rho^2) = 0.43$ at long times. An analysis of the population as a function of time (Fig. 8) reveals population transfer processes for $t > 0.25$. However, there is some population transfer even at shorter times while decoherence is ongoing. Note also, as above, the harmonic case decoheres far slower than the anharmonic Morse oscillator.

One comment is in order regarding the accuracy of the computation. Note that the population of the third state at time $t = 0$ is 0.54. This value should be 0.6 since this is the initial state that we prepared. This difference provides a measure of the numerical error in the individual density matrix elements due to the complexity of the calculation and the oscillating integrand in Eq. (18). Typical errors in the individual ρ_{ij} are on the order of ∼10%–15% with the larger error seen when the states involved are more oscillatory, i.e., superpositions with higher energies. By contrast, the error in the calculation of the purity is significantly smaller; for all cases studied it does not exceed 3%.

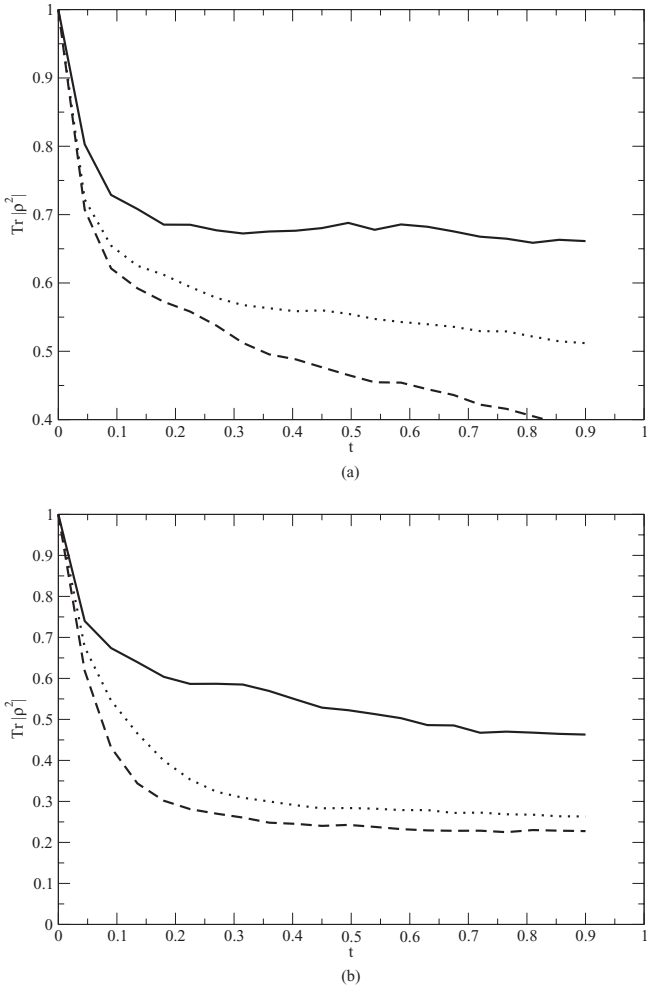

FIG. 7. (a) $\mathrm{Tr}(\rho^2)$ for a harmonic oscillator in a LJ bath as a function of time for three different initial superposition states: 8,9 (solid line); 8,11 (dotted line); and 8,13 (dashed line). (b) $\mathrm{Tr}(\rho^2)$ for a Morse oscillator in a LJ bath as a function of time for three different initial superposition states: 8,9 (solid line); 8,11 (dotted line); and 8,13 (dashed line).

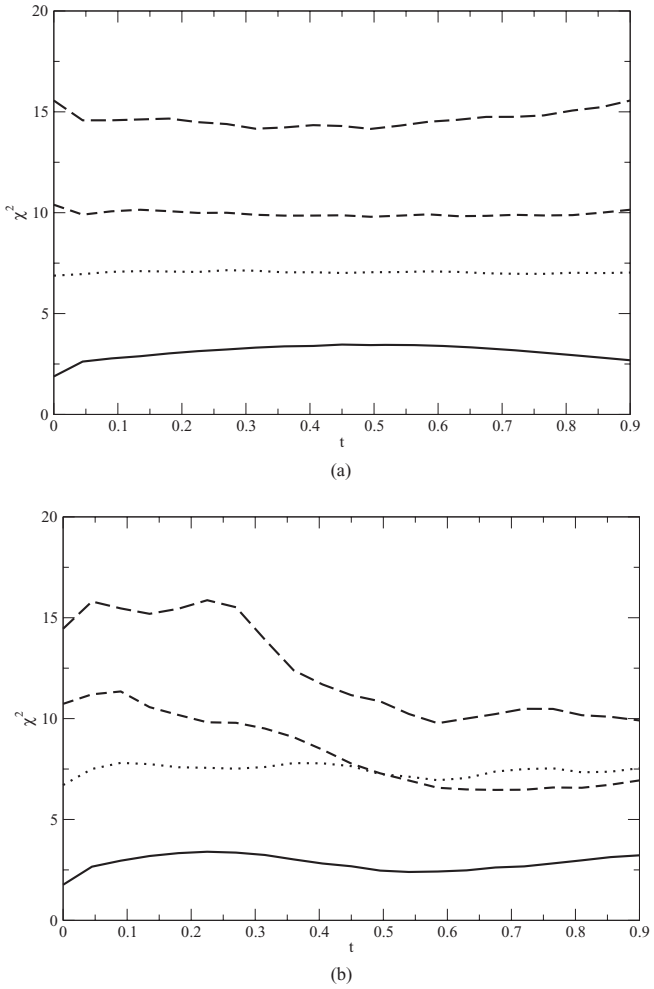

FIG. 9. (a) χ^2 as a function of time for four initial superposition state and the harmonic potential: 0,1 (solid line); 0,3 (dotted line); 0,5 (short dashed line); and 3,6 (long dashed line). Multiply χ^2 by 1.498×10^{45} to obtain the result in units of $\mathrm{J}^{-1}\ \mathrm{Kg}^{-1}$. (b) χ^2 as a function of time for four initial superposition states for the I_2 Morse potential: 0,1 (solid line); 0,3 (dotted line); 0,5 (short dashed line); and 3,6 (long dashed line). Multiply χ^2 by 1.498×10^{45} to obtain the result in units of $\mathrm{J}^{-1}\ \mathrm{Kg}^{-1}$.

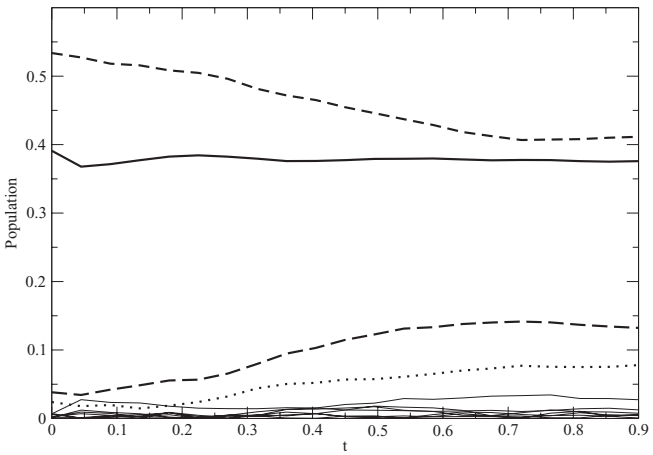

FIG. 8. Population as a function of time for the 0,3 initial superposition state of the Morse potential: $|0\rangle$ (solid line); $|2\rangle$ (dotted line); $|3\rangle$ (short dashed line); and $|4\rangle$ (long dashed line). All other lines are states with populations lower than 0.1 for all times.

The behavior of the individual density matrix elements shows that coherence is retained in individual elements even though on average the system has fully decohered.

C. Caldeira-Leggett

Equation (21) is used to calculate the value of $\chi^2(t)$ for some of the cases presented here. The results for the representative set of superpositions $\{(\psi_1, \psi_2)\} = \{(0, 1); (0, 3); (0, 5); (3, 6)\}$, are presented in Fig. 9. Since these calculations are extremely time consuming compared to the other calculations in this study [due to the large number of sums and integrals in Eq. (21)], these calculations were only performed on the superpositions whose initial states have low-lying energies (up to the superposition 0,3). The time-dependence of χ^2 is quite remarkable insofar as, for all the cases studied, χ^2 is approximately constant in time. The results obtained for $\chi^2(t)$ allow us to estimate a value for D using Eq. (22) and these values, for the same set of superpositions is shown in

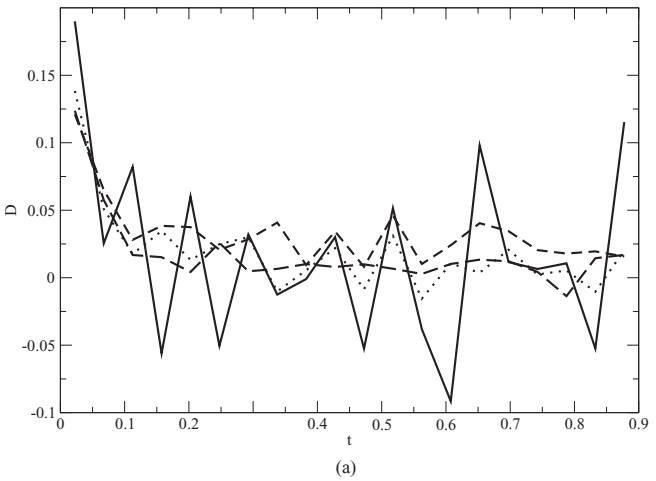

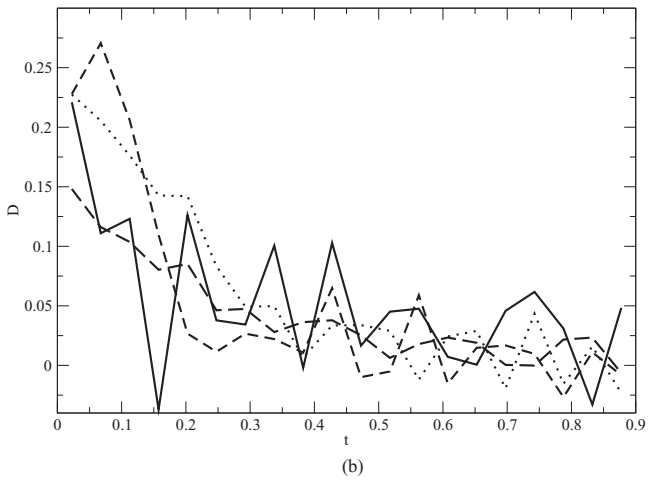

FIG. 10. (a) D as a function of time for four initial superposition states and the harmonic potential: 0,1 (solid line); 0,3 (dotted line); 0,5 (short dashed line); and 3,6 (long dashed line). Multiply D by 2.013×10^{-34} to obtain the result in units of J Kg s^{-1}. (b) D as a function of time for four initial superposition states for the I_2 Morse potential: 0,1 (solid line); 0,3 (dotted line); 0,5 (short dashed line); and 3,6 (long dashed line). Multiply D by 2.013×10^{-34} to obtain the result in units of J Kg s^{-1}.

Fig. 10. Clearly, we do not obtain a constant D, as a consequence of the fact that the Renyi entropy in Eq. (22) is not linear in time. The results for χ^2 and D in the Morse and harmonic I_2 cases, are qualitatively similar, however, there are also significant differences. On one hand, χ^2 is more constant for the harmonic, which is to be expected. The oscillatory nature of the Harmonic oscillator is more symmetric and hence, the phase space structure changes less with time. Clearly, then, the assumptions inherent in the Caldeira-Leggett[26] equations are not applicable for this physical scenario.

Note that the Caldeira-Leggett model was not found useful in our previous tests of I_2 coupled to an harmonic bath[18] under realistic conditions, even though this model arose as a means of modeling such a system. However, it is clear that the various auxiliary conditions (such as high temperature and low coupling) required in deriving this approach are not satisfied in these cases.

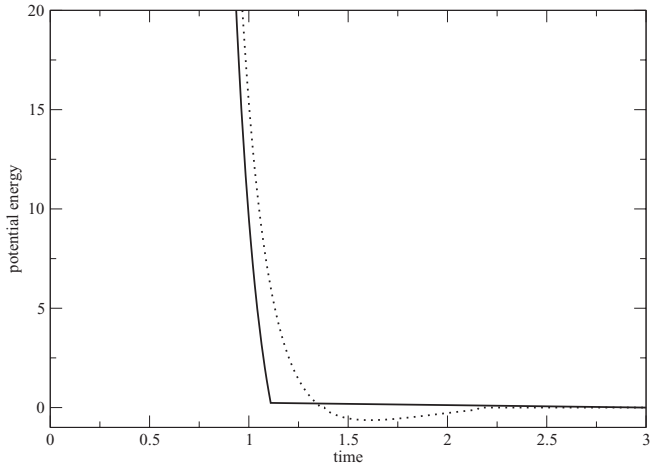

FIG. 11. Example of the LJ potential between the I_2 molecule and a bath particle in a model consisting of: 8 bath particles (solid line) and 23 bath particles (dotted line).

D. Dependence on the number of bath particles

Computations with 864 particles are time consuming. To this end, we examined the possibility of computing decoherence using smaller numbers of bath particles. Results were reasonable for baths as small as $N = 23$ xenon atoms. At first glance, it is unexpected that such a small number of bath particles can accurately reproduce physical properties of a real system. Nevertheless, an analysis of the potentials involved suggest that such computations may be sensible. Figure 11 shows, as an example, the LJ potential between the I_2 diatom and one of the bath particles. While the familiar LJ curve can be seen when the bath is comprised of 23 particles, the curve obtained when the bath is comprised of eight particles is evidently non-physical. Since the MD simulation imposes a potential cutoff that is proportional to the size of the box (when the density of particles is constant), there is a certain distance, r_0 , where the potential is abruptly, unphysically "cut off" and forced to zero. With 23 particles $r_0 \approx 2.25$ and therefore the effect of the cutoff on the calculation is negligible, whereas for the case where the bath contains eight particles, $r_0 \approx 1.13$ and the calculation is incorrect.

Consider now, whether a model bath containing 23 particles can actually reproduce the 864 bath particle results. An example comparing $\mathrm{Tr}(\rho^2)$ for $N = 23$ with that of $N = 864$ bath particles for the cases of the (0,1) superposition and the (0,5) superposition is shown in Fig. 12. While the results for $N = 864$ and $N = 23$ agree completely for the (0,1) superposition, those obtained for the (0,5) superposition differ substantially at $t > 1.3$ ps. Similar results were obtained with many other cases presented in this study: the $N = 23$ results agree with the N = 864 for superpositions of states that are not widely separated in energy and differ at longer times for those superpositions that are initially widely separated in energy. The difference at long times of widely separated initial superposition states can be explained by the fact that the timescale of decoherence is much smaller, and we postulate that the immediate neighbors of the diatom dominate the energy transfers that are important in the decoherence process.

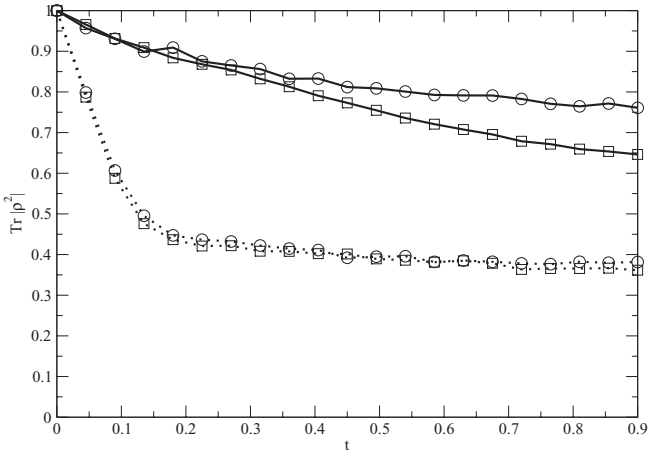

FIG. 12. Comparison of $\mathrm{Tr}(\rho^2)$ for a Morse oscillator in a LJ bath as a function of time for two different initial superposition states: 0,1 (solid lines) and 0,5 (dotted lines) using 23 bath particles (squares) and 864 bath particles (circles).

The short time reliability of the $N = 23$ computation of $\mathrm{Tr}(\rho^2)$ is encouraging, implying much less computer overhead than previously expected if short time trends are desired. Similar results are seen of two individual matrix elements. For example, Fig. 13 shows the decoherence time of sample matrix elements from two different superpositions, (0,3) and (3,6), with $N = 864$ and $N = 23$ bath particles, and the populations of two different levels during the decoherence.

E. Comparison to results obtained with a model system

Very often, decoherence studies do not use MD simulations of the bath to analyze decoherence processes. Instead, models are employed where the bath is described using a few oscillators to generate a desired spectral density. Such a study was done in a semiclassical study of a model system of I_2 that was linearly coupled to a harmonic bath.[18] The main findings of that study agree with those of this paper. In Ref. 18, it was found that decoherence can show non-exponential decay; decoherence is slower if the system's low energy states are initially populated, and occurs rapidly for initial superposition states. The off-diagonal matrix elements were found to "collapse" to the diagonal as the system loses its coherences, with decoherence occurring faster for coherences between levels that are more energetically separated. As mentioned, these observations have been confirmed in the current study. There are however two main differences. First, and significantly, the timescale of decoherence in the current study is much slower than those observed in the harmonic bath model. Second, the behavior of χ^2 and D differ: in Ref. 18, constant values of χ^2 were obtained only for coherent states (as opposed to the constant values of χ^2 obtained in this study), and the resulting values of D varied widely. We note however, that at least with respect to orders of magnitude and short times we can see that both the linear coupling model and the real physical scenario have approximately the same range of values for χ^2 and D. Regarding the difference in the behavior of χ^2 and D, we suggest that in physical reality, the bath may serve to

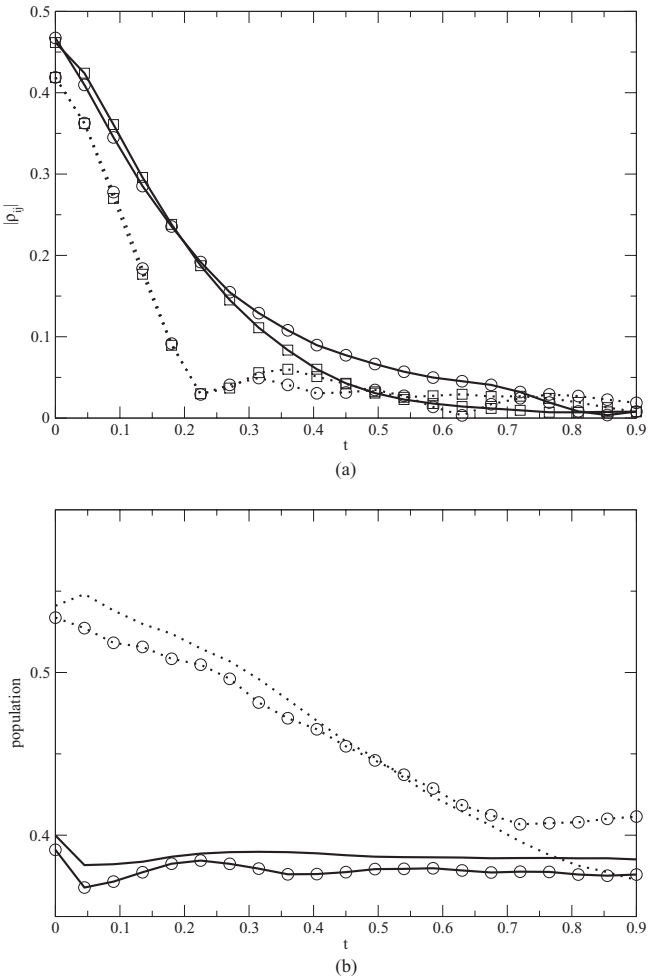

FIG. 13. (a) $|\rho_{i,j}|$ for a Morse oscillator in a LJ bath as a function of time for $i, j = 0, 3$ for the 0,3 superposition (solid line) and $i, j = 3, 6$ (dotted line) for the 3,6 superposition using 23 bath particles (circles) and 864 bath particles (squares). (b) Population for a Morse oscillator in a LJ bath as a function of time for the 0,3 superposition: level 0 (solid line), level 3 (dotted line) using 23 bath particles (no symbol) and 864 bath particles (circles).

preserve the phase space structure of the system for the short time scale of decoherence, resulting in constant values of χ^2. This effect is not shown when the bath is approximated with a spectral density. Future studies of decoherence where the bath is modelled using MD simulations may help clarify the issues raised in this section.

V. SUMMARY

In this paper, we have studied the decoherence of a vibrating diatomic (I_2) in a LJ bath (xenon), using both harmonic and Morse potentials for the system, where we chose for the initial state of the system both coherent states and superposition states. Instead of a theoretical treatment using master equations we utilized a recent quantum-classical correspondence principle, which we proved to be equivalent to the semiclassical linearized IVR treatment and through this, implemented a classical Wigner approach that is much more efficient than the usual LSC-IVR calculations. The efficiency of this method allowed a study of a real "physical" scenario with 864 bath particles. One of the benefits of this calculation

was to show that although for relaxation processes this large number of particles is important in order to obtain accurate rates, if one is interested in decoherence processes at short times, as is often the case, as little as 23 bath particles are sufficient. If, however, one is interested in individual density matrix elements, the results should be taken with some caution, since the error can be considerable.

We found that the rate of decoherence varies greatly when the system potential is even slightly anharmonic. Decoherence also occurs much more rapidly for superposition states compared to coherent states, due to the initial interference structure of these states. It was found that the off-diagonal matrix elements "collapse" to the diagonal as the system loses its coherences, with decoherence occurring faster for coherences between levels that are more energetically separated.

The Caldeira-Leggett approach to decoherence assumes a theoretical model of a system coupled to a bath with a certain spectral density. This analysis, which is widely used leads to certain constraints on various decoherence phenomena, such as the exponential decay of the purity. This work shows that in a real "physical" scenario, the Caldeira-Leggett assumptions are not obeyed. Specifically, no exponential decay of the purity is observed. Despite this, useful information can be obtained for Caldeira-Leggatt variables, that can be calculated using the methods described herein.

ACKNOWLEDGMENTS

This research was supported by the Natural Sciences and Engineering Research Council of Canada.

APPENDIX: RELATION TO THE LSC-IVR

The time correlation function that appears in Eq. (11) (which physically corresponds to the time-evolved density):

$$D(t) = \int dx_s' dx_B' \delta(x_s'(t) - x_s)\rho(x_s, x_B', 0) \tag{A1}$$

can be rewritten in the following manner:

$$D(t) = \int d\mathbf{q}_0' d\mathbf{p}_0' A_w(\mathbf{q}_0', \mathbf{p}_0') B_w(\mathbf{q}_t', \mathbf{p}_t'), \tag{A2}$$

where the definitions $\{\mathbf{q}_0', \mathbf{p}_0'\} \equiv \{x_s', x_B'\}$ (note that the equivalence is between the sets of variables, however, $\mathbf{q}_0' \neq x_s'$ and $\mathbf{p}_0' \neq x_B'$; in particular, $\mathbf{q}_0'$ denotes the position variables of both the system and the bath and $\mathbf{p}_0'$ denotes the momentum variables of both the system and the bath), and the definitions

$$\begin{aligned} A_w(\mathbf{q}_0', \mathbf{p}_0') &\equiv \rho(x_s, x_B', 0), \\ B_w(\mathbf{q}_t', \mathbf{p}_t') &\equiv \delta(x_s'(t) - x_s), \end{aligned} \tag{A3}$$

have been employed. Equations (A1) and (A2) are the well-known linearized semiclassical LSC-IVR expression for a time-correlation function corresponding to the quantum correlation function:

$$D(t) = \mathrm{Tr}(\widehat{A} e^{i\widehat{H}t/\hbar} \widehat{B} e^{-i\widehat{H}t/\hbar}). \tag{A4}$$

We note that writing the LSC-IVR in the form of Eqs. (14) and (13) simplifies its computation, since the integrand does not contain the phase factor that usually appears in such calculations [cf. Eq. (44) in Ref. 18]. Hence, the convergence of the integration is much quicker and demands a much smaller number of classical trajectories. The LSC-IVR calculation was performed for the model described in Ref. 18 using the "box" method described here and the method described in Ref. 18. Exact agreement was established between the two methods, however only 100000 trajectories where used for the method described here, while the method described in Ref. 18 required 64×10^6 trajectories to achieve the same convergence.

[1] W. H. Zurek, Phys. Today **44**, 36 (1991); for an alternative approach to classical-quantum correspondence, see J. Wilkie and P. Brumer, Phys. Rev. A **55**, 27 (1997); **55**, 43 (1997).
[2] W. H. Miller, J. Chem. Phys. **136**, 210901 (2012).
[3] J. S. Briggs and A. Eisfeld, Phys. Rev. E **83**, 051911 (2011).
[4] M. A. Schlosshauer, *Decoherence and the Quantum-to-Classical Transition* (Springer-Verlag, Berlin, 2007).
[5] M. A. Nielsen and I. L. Chuang, *Quantum Computation and Quantum Information* (Cambridge University Press, Cambridge, 2002).
[6] M. Shapiro and P. Brumer, *Quantum Control of Molecular Processes* (Wiley-VCH, Weinheim, 2012).
[7] S. A. Rice and M. Zhao, *Optical Control of Molecular Dynamics* (John Wiley, New York, 2000).
[8] M. Shapiro and P. Brumer, Adv. At., Mol., Opt. Phys. **42**, 287 (2000).
[9] H. Han and P. Brumer, J. Chem. Phys. **122**, 144316 (2005).
[10] A. S. Sanz, Y. Elran, and P. Brumer, Phys. Rev. E **85**, 036218 (2012).
[11] G. S. Engel, T. R. Calhoun, E. L. Read, R.-K. Ahn, T. Mančal, Y.-C. Cheng, R. E. Blankenship, and G. R. Fleming, Nature (London) **446**, 782 (2007).
[12] E. Collini, C. Y. Wong, K. E. Wilk, P. M. G. Curmi, P. Brumer, and G. D. Scholes, Nature (London) **463**, 644 (2010).
[13] L. A. Pachon and P. Brumer, J. Phys. Chem. Lett. **2**, 2728 (2011).
[14] L. A. Pachon and P. Brumer, Phys. Chem. Chem. Phys. **14**, 10094 (2012).
[15] J. von Neumann, *Mathematical Foundations of Quantum Mechanics* (Princeton University Press, Princeton, 1955).
[16] H. P. Breuer and F. Petruccione, *The Theory of Open Quantum Systems* (Oxford, New York, 2002).
[17] R. Zwanzig, Lect. Theor. Phys. **3**, 106 (1960).
[18] Y. Elran and P. Brumer, J. Chem. Phys. **121**, 2673 (2004).
[19] N. Singh and P. Brumer, Faraday Discuss. **153**, 41 (2011).
[20] J. B. Gong and P. Brumer, Phys. Rev. Lett. **90**, 050402 (2003); Phys. Rev. A **68**, 022101 (2003); H. Han and P. Brumer, J. Phys. B **40**, S209 (2007).
[21] For one approach to the classical analog, see C. Jaffé and P. Brumer, J. Chem. Phys. **82**, 2330 (1985); C. Jaffé, S. Kanfer, and P. Brumer, Phys. Rev. Lett. **54**, 8 (1985).
[22] N. Makri, Annu. Rev. Phys. Chem. **50**, 167 (1999); J. Math. Phys. **36**, 2430 (1995).
[23] A. K. Pattanayak and P. Brumer, Phys. Rev. Lett. **79**, 4131 (1997).
[24] S. A. Egorov and J. L. Skinner, J. Chem. Phys. **105**, 7047 (1996).
[25] D. Fraenkel and B. Smit, *Understanding Molecular Simulation* (Academic Press, New York, 2002).
[26] A. O. Caldeira and A. J. Leggett, Physica (Amsterdam) **121A**, 587 (1983); A. J. Leggett, S. Chakravarty, A. T. Dorsey, M. P. A. Fisher, A. Garg, and W. Zwerger, Rev. Mod. Phys. **59**, 1 (1987).